Regular Article

Pradeep Kumar Sahu, Satyaranjan Jena*, Subrat Behera, Madan Mohan Sahu, Soubhagya Ranjan Prusty and Ritesh Dash

Wireless power transfer topology analysis for inkjet-printed coil

https://doi.org/10.1515/eng-2022-0040
received July 08, 2021; accepted April 11, 2022

Abstract: The fabricated inkjet-printed coils (IPCs) are a suitable candidate for near-field wireless power transmission (WPT) to the next generation of high-performance implantable medical devices with extreme size constraints that will target intraocular and intracranial spaces. It is a challenging task for anyone to design an efficient inductive link for power transmission as, the secondary coil (receiver element) is placed 3 mm under the skin surface. This paper focuses on an analytical comparison among the basic four topologies of the WPT system in terms of compensation requirement and power efficiency. Hence, designers can choose the best possible topology depending on the coupling coefficient, coil design, and load impedance. In this work, the printed coil is designed with 10 layers of 10 μm thickness, respectively, in both cases. The effect of IPCs on the secondary side is briefly analyzed by considering the parasite resistance of the coil for compensation; the behavior of the system is not significantly affected by using the printed coils for compensation on the primary side. As the compensating capacitance does not depend on the parasite resistance, the series–series topology is preferable for the WPT system. The efficiency decreases due to the presence of parasite resistance in the printed coils. Moreover, it is required to choose an efficient topology as the efficiency varies from 56% to only 38%.

Keywords: wireless power transmission, inkjet printed coil, compensation, parasite resistance, power transfer efficiency

1 Introduction

Wireless power transmission (WPT) of microelectronic implantable devices has attracted much attention for clinical application. The primitive method of power supply for implanted devices was to insert power cables through skin holes. However, these intrusive methods create a risk of infection through the skin holes. Hence, WPT is suitable for implanted devices because it is more robust and relatively safer. Nowadays, most of the research has been focused on the near-field approach because of the simple design and easy implementation of an inductive link between on-body and in-body transceivers such as Radio-frequency identification links, stimulation devices, and pacemakers. Many modern implants like cochlear and retinal implants, neutral recording and electrical stimulation of muscle devices, and pacemakers still employ batteries [1,2]. However, power transfer through inductive coupling for battery less implantable devices has attracted much attention from the researcher community.

Wireless power transfer from the primary side to the secondary side of the inductive link generally uses the resonant structure [3]. However, due to the presence of tissues in the body and coil misalignment, the biomedical implant uses loosely coupled inductive links with a coupling factor of 0.05 [4]. Hence, there is a limited range of power transfer efficiency.

So far, thin wires using sophisticated winding machines are used for the fabrication of both the coils in the WPT system [5]. However, the next-generation high-performance implantable devices demand a much smaller footprint that must have potential on-chip or on package-level integration

* **Corresponding author: Satyaranjan Jena,** School of Electrical Engineering, KIIT Deemed to be University, Bhubaneswar, India, e-mail: srj.kiit@gmail.com
Pradeep Kumar Sahu: School of Electrical Engineering, KIIT Deemed to be University, Bhubaneswar, India, e-mail: pksahu.nitrkl@gmail.com
Subrat Behera: School of Electrical Engineering, KIIT Deemed to be University, Bhubaneswar, India, e-mail: sbeherafel@kiit.ac.in
Madan Mohan Sahu: Engineering Department, Electrical Division, AIIMS Bhubaneswar, Bhubaneswar, India, e-mail: sahu.mdn@gmail.com
Soubhagya Ranjan Prusty: School of Electrical Engineering, KIIT Deemed to be University, Bhubaneswar, India, e-mail: soubhagya.prustyfel@kiit.ac.ins
Ritesh Dash: School of Electrical and Electronics Engineering, REVA University, Bangalore, India, e-mail: rdasheee@gmail.com

and higher geometrical precision. Keeping in mind the above-mentioned issues, coils with printing technology are suitable for implantable medical devices. Both digital and analog printing technologies are available for printing conductive materials on different substrates [6,7]. The well-developed printing technologies such as offset, gravure, and flexographic printing use printing patterns like differences in wetting, surface relief (recesses), and surface relief (raised) in printing master, respectively. However, masterless inject-printed coils (IPCs) use droplet-size conductive materials and the size is decided by the nozzle diameter and waveforms [8,9]. This balanced technology has a high resolution on thin layers with automated process control. This paper presents the feasibility study of IPC for implantable device applications.

The inkjet printing technique has already been used in a few biomedical applications. Here, inkjet-printed electrodes are used for surface electromyography. These electrodes permit the steps for manufacturing low-impedance conductive tracks with high-density surface electromyography [10]. These technologies are also used to manufacture other biopotential recordings like electrocardiograms and electroencephalograms.

The design of implantable antennas with compact size, isolation from, and comfortability to the human body is a challenging task for WPT systems [11]. Nowadays, flexible biocompatible coils are also used in some biomedical applications, which may create a revolution in the current medical implanted devices. In recent years, these printed electronics dominated over the conventional silicon-based technologies due to their low cost, simple design, light weight, and flexible features with large surface area [12]. It is estimated that the revenue of the flexible electronics market may reach over 300 billion USD by 2028 [13].

The behavior of the WPT system can be extensively studied previously and assessed based on the following parameters: (a) compensations required for desirable frequency [14,15] and (b) power transfer efficiency [16,17]. However, few works of literature are available to address the above-mentioned factors in wireless power transfer systems. Therefore, it appeared reasonable to address an extensive study on the printed coils and loosely coupled inductive link of the inductively coupled power transfer (ICPT) systems. Various ICPT topologies are briefly analyzed on the basis of compensation requirements and power transfer efficiency.

The paper is structured as follows. Section 2 reviews the basic theory of operation for WPT, design, and characterization of inductive links. The detailed methodology for resonant inductively coupled system analysis is described in Section 3. Section 4 explains the analytical comparison based on an inductive wireless power transfer system for biomedical devices by using a combination of closed-form equations in MATLAB (MathWorks) and verification in finite-element analysis tools in HFSS (Ansoft, Pittsburgh, PA), followed by concluding remarks.

2 Characterization of IPCs

In the wireless power system, the concept of an inductive coupling-based WPT system can be realized by using near-field coupled inductive coils. Among various available designs, the system includes at least two closely coupled coils with respect to the coil diameters. Even though three or four coils systems are reported in ref. [18], the two-coil configuration is suitable for the WPT system due to its simplest design, easy control, and easy positioning.

2.1 Principles of ICPT

In a simple WPT design, two magnetically coupled inductive coils are placed in close proximity. This concept is demonstrated in Figure 1. Here, two coils are coupled with each other so that the transmitting coil (primary) transfers energy to the receiving coil (secondary) through the magnetic field. It consists of a pair of coils of inductances L_1 and L_2, which are magnetically coupled by a mutual inductance M. By neglecting the coils' parasitic capacitance, it becomes a non-resonant system. Generally, non-resonant inductively coupled topologies are not suitable for WPT applications due to their poor efficiency compared to the resonant configuration [17].

The resonant topology, also known as near-field resonant inductive coupling (NRIC) [19], can be implemented

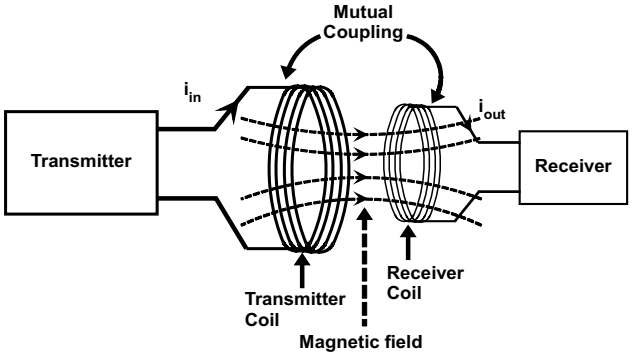

Figure 1: Overview of the ICPT system.

by including capacitors either in series or parallel with the inductive coils. This topology has more efficiency in contrast to the non-resonant system. The NRIC of the two-coil configuration has four possible arrangements, which are shown in Figure 2. In each arrangement, the coil is connected with a capacitor so that both sides of the magnetic link constitute a resonant circuit. Each arrangement shown in Figure 2 is treated as a two-port network.

The parameters like impedance and the gain of the magnetic link can be measured by using circuit analysis for any topologies shown in Figure 2, which are reported in ref. [20]. Depending on the driver, the link gain can be expressed either as a trans-impedance (v_o/i_{in}) or as a voltage gain (v_o/v_{in}). Here, v_{in}, v_o, and i_{in} are the input voltage, output voltage, and input current of the ICPT system, respectively. This analysis is further investigated in ref. [18]. Here, the optimization schemes and link efficiency expressions are derived for the WPT system. The elementary analysis such as circuit parameters, extracting parameters like power transfer efficiency, and the power transfer capability for an inductive link can be carried out by combining these analyses. The detailed design procedures of the WPT system are briefly analyzed in the next section.

2.2 Characterization

The four different ICPT topologies can be characterized by comparing simulation and analytical results. The detailed characterization procedures are reported in ref. [20]. The design coil parameters are given in Table 1. Here, Model 1 and Model 2 are the two different materials of subtractive etching and IPCs, respectively.

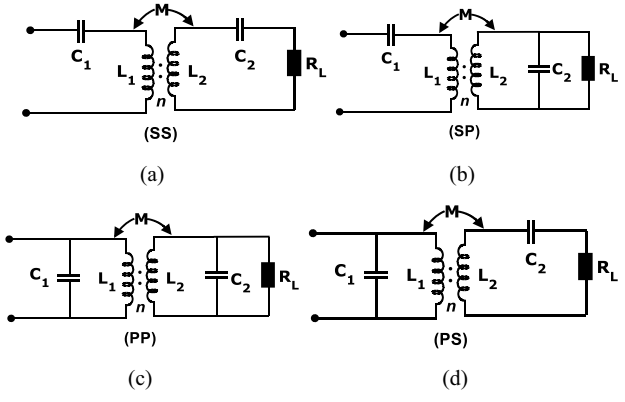

Figure 2: Comparison of near-field coupling topologies: (a) series–series (SS), (b) series–parallel (SP), (c) parallel–parallel (PP), and (d) parallel–series (PS).

Table 1: Nature of coil

Name	Coils	Substrate	Materials
Model – 1 [6] (M–1)	Subtractive etching	FR4 (0.8 mm)	Copper
Model – 2 [21] (M–2)	Inkjet printed	Kapton (127 μm)	Silver ink (10 μm–10 layers)

From the table, it is seen that all four topologies have the same inductance value whereas both input resistance and thus quality factor have a significant change in value for all arrangements. This is because the conductive track of the coil has different thicknesses and conductivities. Table 2 presents the selected conductivities for four topologies.

From the table, it is observed that the printed coil has lower conductivity than the subtractive etching design. Hence, the printed design coil has relatively higher resistance. Unlike the subtractive etching design, the conductivity of the printed coil can be adjusted by modifying the sintering process. By using the printed coil technique, the thickness of the printed layers can be varied by 1 μm in resolution. Changing the track thickness will affect both the quality factor and input resistance of the coil, as the coil thickness is inside the skin depth. Both the Q-factor and input resistance cannot be adjusted for the coil thickness deeper than the depth of the skin [20].

By maintaining the same coil inductance value for all four topologies, a coil antenna can be designed via a printed coil with a small quality factor of 10.3 [20]. The printed coil is designed with 10 layers, each having a thickness of 10 μm. Again the compensating capacitance does not depend on the parasite resistance of the coils.

3 Methodology

The WPT system consists of four possible topologies (shown in Figure 2) and is used to transmit power from the transmitting coil (primary) to receiving coils. These topologies are interpreted as SS/SP/PS/PP, where the type of compensation for the primary or transmitter coil is represented by the first letter and that for the secondary or receiver side is represented by the second letter. Here, S and P stand for series and parallel topologies, respectively. The primary- and secondary-side parameters are denoted by sub-indexes 1 and 2, respectively. Here, the mutual inductance and the coupling factor are represented

Table 2: Parameter of coil

Name	Coil resistance (Ω)	Coil inductance (μH)	*Q*-factor	Conductivity (S/m)
Model – 1 [6] (M–1)	2	2.8	119.2	59.6×10^6
Model – 2 [21] (M–2)	23	2.8	10.3	8×10^6

by symbols M and k, respectively. L_1, C_1, R_1 and L_2, C_2, R_2 are the self-inductance, capacitance and internal resistance of the primary side and secondary side, respectively. Ω and R_L are the angular frequency and load resistance, respectively.

The phasor model of a typical magnetically coupled WPT system is illustrated in Figure 3. Assuming the steady-state condition and sinusoidal supply voltage, the phasor model of the system can be developed by considering its equivalent impedance. The total impedance of the system is characterized by the reflected impedance Z_r, as shown in Figure 3(c):

$$Z_r = \frac{M^2\omega^2}{jL_2\omega + R_L} = \frac{M^2\omega^2}{Z_2}, \tag{1}$$

Here, Z_1, Z_2, and Z_r are the primary-side, secondary-side and reflected impedances, respectively. Similarly, the primary- and secondary-side current are represented by I_1 and I_2, respectively. The secondaryside equivalent impedance (Z_2), as referred to the secondary voltage generator ($jM\omega I_1$), is the denominator of the reflected impedance, as shown in Figure 3(b). Assuming the secondary circuit with the resonance condition, different reflected impedances are observed for different types of compensation.

(1) Secondary side with series compensation:

$$Z_2 = j\omega L_2 + R_L + \frac{1}{j\omega C_2}. \tag{2}$$

(2) Secondary side with parallel compensation:

$$Z_2 = j\omega L_2 + \frac{1}{j\omega C_2 + \frac{1}{R_L}}. \tag{3}$$

The equivalent impedance, as referred to the primary side is represented by Z_1, and its value depends on the type of the primary-side topology.

(1) Primary side with series compensation:

$$Z_1 = j\omega L_1 + z_r + \frac{1}{j\omega C_1}. \tag{4}$$

(2) Primary side with parallel compensation:

$$Z_1 = \frac{1}{j\omega C_1 + \frac{1}{j\omega L_1 + Z_r}}. \tag{5}$$

The behavior of each topology can be briefly studied by analyzing the impedance expressions of Z_r and Z_1. In this section, the performance of the WPT system can be evaluated on the basis of four main parameters such as compensation, bifurcation phenomenon, maximum power transfer efficiency, and power transfer capability.

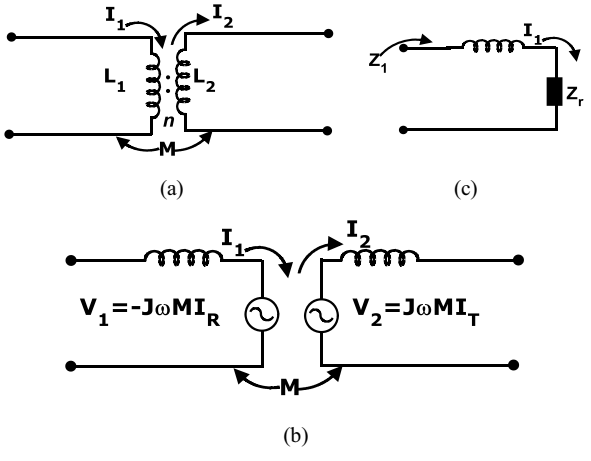

Figure 3: ICPT system phasor model: (a) inductive coupling circuit, (b) equivalent circuit, and (c) reflected impedance referred to the primary side.

3.1 Compensation

Both primary and secondary sides of the WPT system should be operated at the same resonating frequency in order to provide efficient power transfer. Since the primary side is affected by the secondary side, the reactance component of reflected impedance Z_r should be compensated by the primary side. The size of the primary side capacitor can be determined by using the conditions as

$$\mathrm{Im}\{Z_1\}|_{\omega=\omega_0} = 0, \tag{6}$$

where ω_0 represents the secondary-side resonance frequency:

$$\omega_0 = \frac{1}{\sqrt{L_2C_2}}. \tag{7}$$

3.2 Power transfer efficiency

The performance of an inductive link can be quantified by a crucial parameter; the power transfer efficiency [16,17] is expressed as the ratio of the energy available across the load to the total supply voltage in one cycle. Due to the presence of parasite resistance in the coils, the inductively coupled circuit suffered from the energy losses, which are briefly discussed in the next section.

The overall efficiency of the WPT system is not affected by the primary-side compensation, which is reported previously in ref. [16]. Hence, only two topologies; SS and SP are studied briefly in this paper as these topologies are equivalent to PS and PP, respectively. The detailed procedure for developing the related equations for SP topology as a case study is briefly studied in this section. Similarly, for the SS topology, the same procedure may be followed which is not discussed here. The efficiency of the WPT system can be determined by developing its phasor model, which is shown in Figure 3.

The determination of the overall efficiency of the WPT system is carried out in two steps. The primary-side efficiency (η_1) is calculated first by taking the ratio between the power delivered to the reflected impedance and the supply power from the source:

$$\eta_1 = \frac{\mathrm{Re}\{V_{Z_r} I^{\star}_{Z_r}\}}{\mathrm{Re}\{V_{\mathrm{in}} I^{\star}_{\mathrm{in}}\}}, \tag{8}$$

where V_{Z_r} and I_{Z_r} are voltage and current through the reflected impedance, whereas V_{in} and I_{in} are the input voltage and current through the primary coil, respectively.

Then, the secondary-side efficiency (η_2) is calculated using the following equation:

$$\eta_2 = \frac{\mathrm{Re}\{V_{R_L} I^{\star}_{R_L}\}}{\mathrm{Re}\{V_2 I^{\star}_2\}}. \tag{9}$$

Here, V_2 and $I^{\star}_2$ are the induced secondary-side voltage and current, whereas V_{R_L} and $I^{\star}_{R_L}$ are the voltage and current available at load, respectively.

The overall efficiency of the ICPT system can be derived by multiplying the efficiencies of both the primary and secondary sides as shown in equations (8) and (9).

$$\eta = \eta_1 \eta_2. \tag{10}$$

The detailed methodology of the topology analysis is briefly discussed in the next section. This analysis is carried out on the basis of primary side compensation issues, power transfer efficiency, bifurcation analysis, and power transfer capability. Unlike etched copper antennas, the printed one has considerable parasite resistance which cannot be neglected. Therefore, the analysis is carried out by taking parasite resistance into account. The influence of designing secondary coil through printed technology is briefly discussed. In all topologies, the design of the primary coil is fixed and the capacitors are designed to operate at a resonant frequency of 13.56 MHz.

4 Compensation analysis

For efficient power transfer, both sides of the coupled circuit should be operated in a single resonant frequency, and the total reactance referring to the primary sides needs to be compensated by adjusting the primary-side capacitance (C_1) [14,15]. This capacitance is calculated by using the following formula:

$$\mathrm{Im}\{Z_1\}|_{\omega=\omega_0} = 0.$$

4.1 Ignoring the parasite resistances of IPCs ($R_1 = 0$, $R_2 = 0$)

Neglecting coil resistances, the calculations of primary side capacitance are given below for different topologies.

(1) SS topology:

$$C_1 = \frac{1}{\omega_0^2 L_1}. \tag{11}$$

(2) SP topology:

$$C_1 = \frac{1}{\omega_0^2\left(L_1 - \frac{M^2}{L_2}\right)}. \tag{12}$$

(3) PS topology:

$$C_1 = \frac{L_1 R_L^2}{\omega_0^2 (M^4 \omega_0^2 + L_1^2 R_L^2)}. \tag{13}$$

(4) PP topology:

$$C_1 = \frac{(L_1 L_2 - M^2) L_2^3}{M^4 R_L^2 + \omega_0^2 L_2^2 (L_1^2 L_2^2 + M^4 - 2 L_1 L_2 M^2)}. \tag{14}$$

From the above expressions it is clearly observed that for all topologies except the SS topology, the capacitance depends on both primary and secondary parameters, i.e., the presence of the coupling coefficient. This coupling coefficient may vary by changing the distance, medium, etc. Also, the coupling coefficient (k) is very poor, which decreases the efficiency. The primary-side capacitors

required to compensate on the secondary side without considering the parasite resistance for different coils are shown in Figure 4.

4.2 Considering the parasite resistances of IPCs

By considering the coil internal resistances, the primary side capacitance is as follows;

(1) SS topology:

$$C_1 = \frac{1}{\omega_0^2 L_1}. \tag{15}$$

(2) SP topology:

$$C_1 = \frac{L_2 C_2 (C_2 R_2 R_L + L_2)^2 + L_2 C_2 R_2^2}{L_1 (C_2 R_2 R_L + L_2)^2 + C_2 L_2 L_1 R_2^2 - L_2 M^2}. \tag{16}$$

(3) PS topology:

$$\begin{aligned} C_1 = {} & L_1 (R_L + R_2)^2 / (R_1^2 (R_L + R_2)^2 \\ & + \omega_0^2 L_1^2 (R_L + R_2)^2 (C_2 R_2 R_L + L_2)^2 \\ & + 2\omega_0^2 M^2 R_1 + (R_L + R_2) + (\omega_0 M)^4). \end{aligned} \tag{17}$$

(4) PP topology:

$$\begin{aligned} C_1 = {} & ((C_2^2 L_1 R_L^2 R_2^2 + 2 C_2 L_1 L_2 R_2 R_L \\ & \times L_1 L_2^2 + C_2 L_1 L_2 R_2^2 - L_2 M^2) C_2 L_2^2) / (A + B + C), \end{aligned} \tag{18}$$

where

$$\begin{aligned} A = {} & C_2^2 L_2 R_2 (C_2 L_2 R_L^2 R_1^2 R_2 + L_1^2 R_L^2 R_2 \\ & + 2 L_2^2 R_1^2 R_L + C_2^2 R_1^2 R_2 + 2 M^2 R_L^2 R_1), \end{aligned} \tag{19}$$

$$\begin{aligned} B = {} & C_2 L_2^2 (2 L_1^2 R_L R_2 + L_1^2 R_2^2 + L_2^2 R_1^2 \\ & + 2 M^2 R_L R_1 + 2 M^2 R_2 R_1). \end{aligned} \tag{20}$$

$$C = M^4 C_2 R_L^2 + L_1^2 L_2^2 - 2 L_1^2 L_2^3 - 2 L_1 L_2^2 M^2 + L_2 M^4. \tag{21}$$

The primary-side capacitors are required to compensate on the secondary side with considering the parasite resistance for different coils are shown in Figure 4. In the SS topology, the capacitor only depends on the primary-side inductance and does not depend on the secondary-side parameter or internal resistance of the coils. So, the SS topology is suitable for the printed coils. On the other hand, the coefficient of coupling k is very small, and the effect of change on the secondary side is negligible on the primary side. So, other topologies are also considered for printed coils for a very less value of k. Otherwise, variations of the primary-side capacitor are required for the compensation [14,15].

5 Power transfer efficiency analysis

The final efficiency only depends on the secondary-side compensation and does not depend on the primary-side compensation [21]. The final efficiencies of SS/PS and SP/PP topologies are given as follows:

$$\begin{aligned} \eta^{SS} = {} & (1 + R_2/R_L + R_1/(k^2 R_L L_1) \\ & \cdot (L_2 + 1/\omega^2 ((R_2 + R_L)^2 / L_2 \\ & - 2/C_2) + 1/(\omega^4 L_2 C_2^2)))^{-1}, \end{aligned} \tag{22}$$

$$\begin{aligned} \eta^{SP} = {} & (1 + R_2/R_L + \omega^2 R_L R_2 C_2^2 + R_2/(k^2 L_2 L_1 R_L) \\ & \times (((1 - \omega^2 L_2 C_2) R_L + R_2)/\omega)^2 + (L_2 + R_L C_2 R_2)^2))^{-1}. \end{aligned} \tag{23}$$

Figure 5 shows the variation of efficiency by varying the receiving-side resistance (R_2) with different load

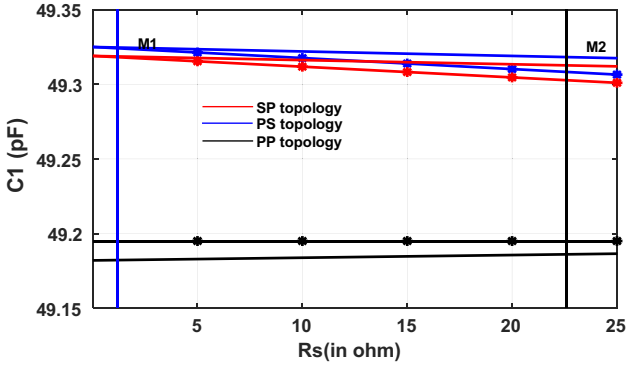

Figure 4: Primary compensation capacitance with the effect of secondary coil resistance R_2. R_L = 50 Ω (no mark) and R_L = 200 Ω (with point marked).

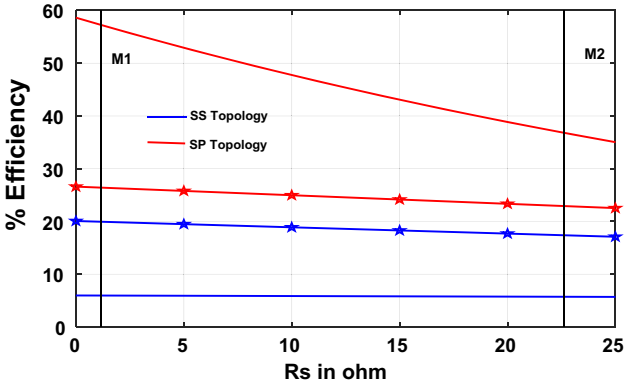

Figure 5: Efficiency vs effect of resistance R_2 at different load: R_L = 50 Ω and R_L = 200 Ω.

impedances. This figure clearly shows that the efficiency of the SP/PP topology is very less compared to that of the PS/SS topology, with low value of secondary side coil resistance. For a higher value of the secondary-side coil resistance, the efficiency decreases for both topologies. In either case, the SS topology gives higher efficiency than the SP topology.

Considering load resistance R_L, series compensation gives higher efficiency in low loads and better efficiency in lower loads with lower values of secondary-side coil internal resistance. However, in the case of parallel compensation, the efficiency will be less in low value of loads and comparatively high efficiency in high loads.

From expressions (22) and (23), it is observed that the efficiency also depends on the operating frequency and coupling coefficient.

Comparing the above two expressions, for the parallel secondary-side compensated topology, the efficiency depends on the higher value of the coupling coefficient "k. As the coupling coefficient is very small and varies due to the variation in distance, angle and person to person, the efficiency will vary in a wide range.

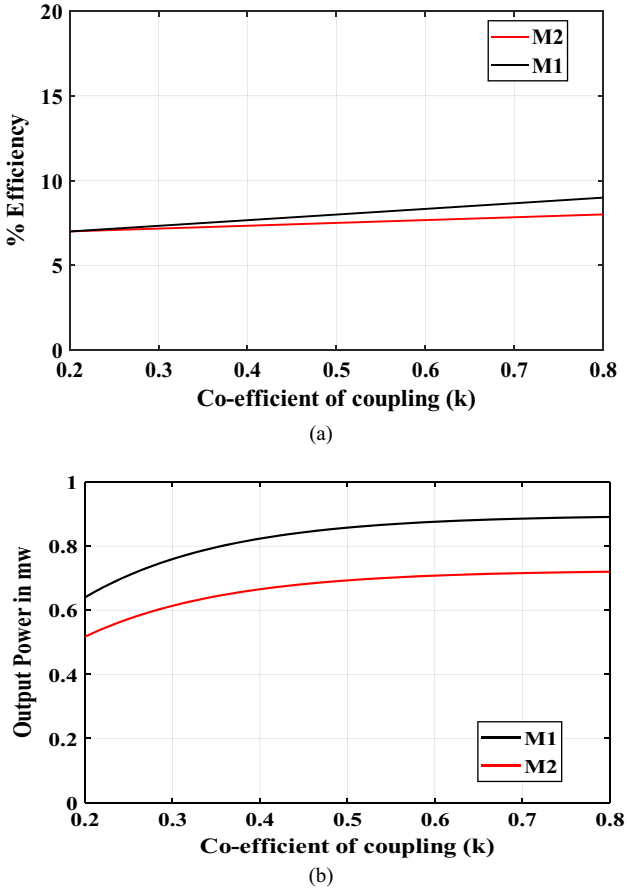

Figure 6: SP/PP topology: (a) change in efficiency with respect to the coefficient of coupling and (b) change in output power with respect to the coefficient of coupling.

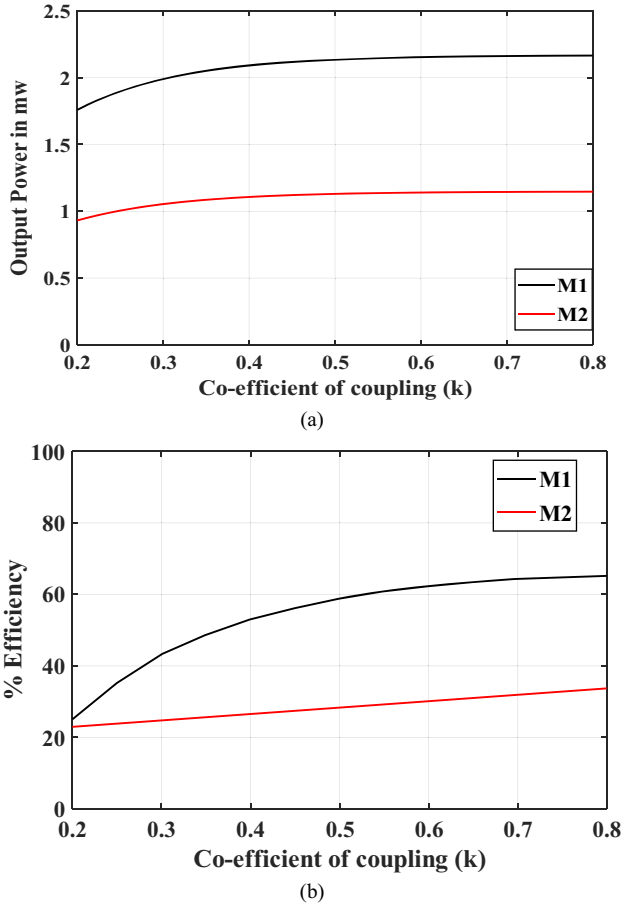

Figure 7: SS/PS topology: (a) change in efficiency with respect to the coefficient of coupling and (b) change in output power with respect to the coefficient of coupling.

The variation of efficiency and output power (in mW) by varying the coupling coefficient for the SP/PP topology is shown in Figure 6(a) and (b). For a large value of k, the efficiency will remain constant and maintain a high value.

Similarly, the variation of efficiency and output power (in mW) by varying the coupling coefficient for the SS/PS topology is shown in Figure 7(a) and (b). In the case of series secondary-side compensated topologies, the efficiency for power transfer is better for even small values of k. Efficiency variation is also very less with the multifrequency operation and the variation of the coupling coefficient.

6 Conclusion

This paper has provided a detailed review of analytic comparisons among the various WPT topologies using a

printed coil for biomedical applications. This study was carried out with the help of a developed phasor model for the loosely coupled inductive link environment and by considering the parasite resistance of the printed coil. Even though the performance of these topologies relies on their final application, specified guidelines and rules were proposed on the basis of compensation requirements, and efficiencies. Out of the various topologies, the primary-side capacitance (C_1) of SS topology is independent of the parasite resistance of the printed coils. Similarly, for the other topologies, the presence of the parasite resistance is not relevant; however, it should be thoroughly checked dep [ending on the characteristics of the application.

Among all four WPT topologies, the SS one attracts attention for medical implanted applications due to its simple design as the capacitance required for compensation is independent of both the coupling factor and the load resistance. This property is required for biomedical applications due to the change in media. It is a challenging task for anyone to maintain a constant angle or distance between external and implanted coils. When the secondary coil uses printed coils, the losses increase (deteriorate efficiency) due to the presence of parasite resistance in the coil. The efficiency of the WPT system in printed coils depends on the output load and topology. As compared to etched copper-based coils, the efficiency of the system using printed coils varies between 56% for the SS topology with a load of $R_L = 50\,\Omega$ and only 38% for the SP topology with a load of $R_L = 200\,\Omega$. Here, the design by considering the parasite resistance of the coils does not affect its performance like; compensation requirement, but its efficiency decreases for the wireless power transfer system.

Conflict of interest: Authors state no conflict of interest.

References

[1] Lee B, Kiani M, Ghovanloo M. A triple-loop inductive power transmission system for biomedical applications. IEEE Trans Biomed circuits Syst. 2015 Feb 4;10(1):138–48.

[2] Lee G, Waters BH, Shin YG, Smith JR, Park WS. A reconfigurable resonant coil for range adaptation wireless power transfer. IEEE Trans Microw Theory Tech. 2016 Jan 11;64(2):624–32.

[3] Guidi G, Suul JA. Minimizing converter requirements of inductive power transfer systems with constant voltage load and variable coupling conditions. IEEE Trans Ind Electron. 2016 Jun 20;63(11):6835–44.

[4] Jegadeesan R, Guo YX. A study on the inductive power links for implantable biomedical devices. 2010 IEEE Antennas and Propagation Society International Symposium. IEEE; 2010 Jul 11. p. 1–4.

[5] Raju S, Wu R, Chan M, Yue CP. Modeling of mutual coupling between planar inductors in wireless power applications. IEEE Trans Power Electron. 2013 Mar 20;29(1):481–90.

[6] Stoppa M, Chiolerio A. Wearable electronics and smart textiles: A critical review. sensors. 2014 Jul;14(7):11957–92.

[7] Hutchings IM, Martin GD, editors. Inkjet technology for digital fabrication. Hoboken, New Jersey, U.S: John Wiley & Sons; 2012 Nov 9.

[8] Goel P, Singh S, Kaur H, Mishra S, Deep A. Low-cost inkjet printing of metal–organic frameworks patterns on different substrates and their applications in ammonia sensing. Sens Actuators B Chem. 2021 Feb 15;329:129157.

[9] Lakafosis V, Rida A, Vyas R, Yang L, Nikolaou S, Tentzeris MM. Progress towards the first wireless sensor networks consisting of inkjet-printed, paper-based RFID-enabled sensor tags. Proc IEEE. 2010 Jul 1;98(9):1601–9.

[10] Gao M, Li L, Song Y. Inkjet printing wearable electronic devices. J Mater Chem C. 2017;5(12):2971–93.

[11] Bahrami H, Mirbozorgi SA, Ameli R, Rusch LA, Gosselin B. Flexible, polarization-diverse UWB antennas for implantable neural recording systems. IEEE Trans Biomed Circuits Syst. 2015 Mar 16;10(1):38–48.

[12] Nayak L, Mohanty S, Nayak SK, Ramadoss A. A review on inkjet printing of nanoparticle inks for flexible electronics. J Mater Chem C. 2019;7(29):8771–95.

[13] Hu J. Overview of flexible electronics from ITRI's viewpoint. 2010 28th VLSI Test Symposium (VTS). IEEE; 2010 Apr 19. p. 84–4.

[14] Wang CS, Covic GA, Stielau OH. General stability criterions for zero phase angle controlled loosely coupled inductive power transfer systems. IECON'01. 27th Annual Conference of the IEEE Industrial Electronics Society (Cat. No. 37243). Vol. 2. Piscataway, NJ: IEEE; 2001 Nov 29. p. 1049–54.

[15] Rajarman R, Alvarado F, Maniaci A, Camfield R, Jalali S. Determination of location and amount of series compensation to increase power transfer capability. IEEE Trans Power Syst. 1998 May;13(2):294–300.

[16] Stielau OH, Covic GA. Design of loosely coupled inductive power transfer systems. PowerCon 2000. 2000 International Conference on Power System Technology. Proceedings (Cat. No. 00EX409). Vol. 1. Piscataway, NJ: IEEE; 2000 Dec 4. p. 85–90.

[17] Ali H, Ahmad TJ, Khan SA. Mathematical modeling of an inductive link for optimizing efficiency. 2009 IEEE Symposium on Industrial Electronics & Applications. Vol. 2. IEEE; 2009 Oct 4. p. 831–5

[18] Mirbozorgi SA, Yeon P, Ghovanloo M. Robust wireless power transmission to mm-sized free-floating distributed implants. IEEE Trans Biomed circuits Syst. 2017 May 19;11(3):692–702.

[19] Terman FE. Radio engineers' handbook. New York and London: McGraw-Hill; 1943 Jan.

[20] Rida A, Yang L, Vyas R, Tentzeris MM. Conductive inkjet-printed antennas on flexible low-cost paper-based substrates for RFID and WSN applications. IEEE Antennas Propag Mag. 2009 Sep 18;51(3):13–23.

[21] Salmerón JF, Molina-Lopez F, Briand D, Ruan JJ, Rivadeneyra A, Carvajal MA, et al. Properties and printability of inkjet and screen-printed silver patterns for RFID antennas. J Electron Mater. 2014 Feb;43(2):604–17.